PRODUCTION OF SECONDARIES IN HIGH ENERGY HEAVY ION COLLISIONS

J. Dias de Deus[1] **and Yu. M. Shabelski**

Petersburg Nuclear Physics Institute, Gatchina, St.Petersburg, Russia

ABSTRACT

In the framework of Quark-Gluon String Model we calculate the inclusive spectra of secondaries produced in heavy ion collisions at intermediate (CERN SPS) and at much higher (RHIC) energies. We demonstrate that the mechanism of secondary production changed drastically in the energy interval $\sqrt{s} = 20-60$ GeV and that is in agreement with qualitative estimates of Glauber-Gribov theory. The results of numerical calculations at intermediate energies are in reasonable agreement with the data. At RHIC energies numerically large inelastic screening corrections should be accounted for in calculations.

PACS. 25.75.Dw Particle and resonance production

E-mail: shabelsk@thd.pnpi.spb.ru

1) CENTRA, Istituto Superior Tecnico, Lisbon, Portugal

1 Introduction

The Quark–Gluon String Model (QGSM) and the Dual Parton Model (DPM) are based on the Dual Topological Unitarization (DTU) and describe quite reasonably many features of high energy production processes, including the inclusive spectra of different secondary hadrons, their multiplicities and multiplicity distributions, etc., both in hadron–nucleon and hadron–nucleus collisions [1]–[7]. High energy interactions are considered as proceeding via the exchange of one or several Pomerons and all elastic and inelastic processes result from cutting through or between Pomerons [8]. Inclusive spectra of hadrons are related to the corresponding fragmentation functions of quarks and diquarks, which are constructed using the Reggeon counting rules [9].

In the case of interaction with nuclear target the Multiple Scattering Theory (Gribov-Glauber Theory) is used and it allows to consider the interaction with nuclear target as the superposition of interactions with different numbers of target nucleons.

In the case of heavy ion collisions the Multiple Scattering Theory also allows to consider this interaction as the superposition of separate nucleon–nucleon interactions. However, in this case there is no possibility to sum up all the diagrams in a rather simple form. The first simple classes of diagrams can be accounted as the simple expressions [10, 11]. The situation with more complicate diagrams is not so clear [12]–[14].

In this paper we present the QGSM results for the calculation of the inclusive spectra of secondaries produced in heavy ion collisions both at intermediate (CERN SPS, $\sqrt{s_{NN}} = 17$ GeV) and much higher (RHIC, $\sqrt{s_{NN}} = 60 - 200$ GeV) energies. The data at GSI and CERN SPS energies [15]-[18] are in reasonable agreement with Multiple Scattering Theory and with QGSM (see more detailed discussion in Section 3). However the similar calculations overestimate the data at RHIC energies by about a factor of two, as shown in Section 4. This effect was explained in [19] as large contribution of inelastic screening correction namely in the case of heavy ion collisions. We estimate the energy region where these correction increase from several percents to twice as $\sqrt{s_{NN}} = 20 - 60$ GeV.

2 Inclusive spectra of secondary hadrons in the Quark-Gluon String Model

For the quantitative predictions we need a model for multiparticle production and we will use the QGSM for the numerical calculations presented below.

As mentioned above, high energy hadron–nucleon and hadron–nucleus interactions are considered in the QGSM as proceeding via the exchange of one or several Pomerons. Each Pomeron corresponds to a cylinder diagram, see Fig. 1a, and thus, when cutting a Pomeron, two showers of secondaries are produced, as it is shown in Fig. 1b. The inclusive spectrum of secondaries is determined by the convolution of diquark, valence quark and sea quark distributions $u(x, n)$ in the incident particles and the fragmentation functions

$G(z)$ of quarks and diquarks into secondary hadrons. The diquark and quark distribution functions depend on the number n of cut Pomerons in the considered diagram.

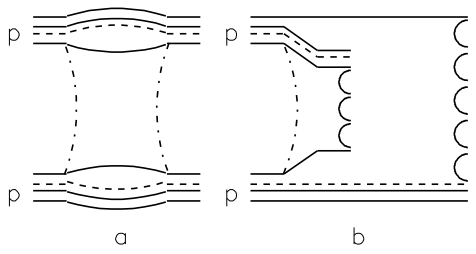

Figure 1: Cylinder diagram (cylinder is shown by dash-dotted curves) corresponding to the one–Pomeron exchange contribution to elastic pp scattering (a) and its cut which determines the contribution to inelastic pp cross section (b). Quarks are shown by solid curves and string junctions [20] by dashed curves.

In the case of a nucleon target the inclusive spectrum of a secondary hadron h has the form [1]:

$$\frac{x}{\sigma_{inel}}\frac{d\sigma}{dx} = \sum_{n=1}^{\infty} w_n \phi_n^h(x) \quad , \tag{1}$$

where the functions $\phi_n^h(x)$ determine the contribution of diagrams with n cut Pomerons and w_n is the probability of this process [21]. Here we neglect the contributions of diffraction dissociation processes which are comparatively small in most of the processes considered below. This diffraction dissociation contribution is important mainly for secondary production in large x_F region, which in not important in the present calculations.

For pp collisions

$$\phi_{pp}^h(x) = f_{qq}^h(x_+,n) f_q^h(x_-,n) + f_q^h(x_+,n) f_{qq}^h(x_-,n) + 2(n-1) f_s^h(x_+,n) f_s^h(x_-,n) \quad , \tag{2}$$

$$x_\pm = \frac{1}{2}[\sqrt{4m_T^2/s + x^2} \pm x] \quad , \tag{3}$$

where f_{qq}, f_q and f_s correspond to the contributions of diquarks, valence quarks and sea quarks, respectively.

They are determined by the convolution of the diquark and quark distributions with the fragmentation functions, for example,

$$f_q^h(x_+,n) = \int_{x_+}^1 u_q(x_1,n) G_q^h(x_+/x_1) dx_1 \quad . \tag{4}$$

The diquark and quark distributions as well as the fragmentation functions are determined from Regge intercepts [9].

In the case of nuclear targets we should consider the possibility of one or several Pomeron cuts in each of the ν blobs of hadron–nucleon inelastic interactions as well as cuts between Pomerons. For example, for a pA collision one of the cut Pomerons links a diquark and a valence quark of the projectile proton with a valence quark and diquark of one target nucleon. Other Pomerons link the sea quark–antiquark pairs of the projective proton with diquarks and valence quarks of another target nucleons and with sea quark–antiquark pairs of the target.

For example, one of the diagram for inelastic interaction with two target nucleons is shown in Fig. 2. In the blob of the pN_1 inelastic interaction one Pomeron is cut, and in the blob of pN_2 interaction two Pomerons are cut. It is essential to take into account every possible Pomeron configuration and permutation in all digrams. The process shown in Fig. 2 satisfies the condition [22]–[25] that the absorptive parts of hadron–nucleus amplitude are determined by the combinations of the absorptive parts of hadron–nucleon interactions.

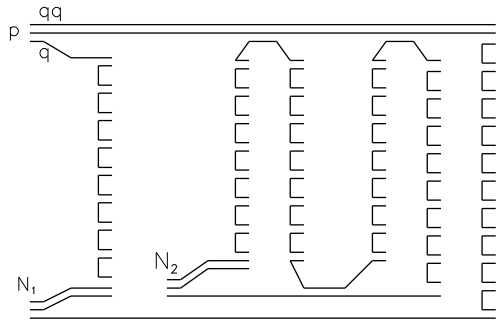

Figure 2: One of the diagrams for inelastic interaction of an incident proton with two target nucleons N_1 and N_2 in a pA collision.

In the case of inelastic interactions with ν target nucleons n be the total number of cut Pomerons in hA collisions ($n \geq \nu$) and let n_i be the number of cut Pomerons connecting with the i-th target nucleon ($1 \leq n_i \leq n - \nu + 1$). We define the relative weight of the contribution with n_i cut Pomerons in every hN blob as $w_{n_i}^{hN}$. For the inclusive spectrum of the secondary hadron h produced in a pA collision we obtain [5]

$$\frac{x_E}{\sigma_{pA}^{prod}}\frac{d\sigma}{dx_F} = \sum_{\nu=1}^{A} V_{pA}^{(\nu)} \left\{ \sum_{n=\nu}^{\infty} \sum_{n_1=1}^{n-\nu+1} \cdots \sum_{n_\nu=1}^{n-\nu+1} \prod_{l=1}^{\nu} w_{n_l}^{pN} \times \right. \tag{5}$$
$$\times \left[f_{qq}^h(x_+,n) f_q^h(x_-,n_l) + f_q^h(x_+,n) f_{qq}^h(x_-,n_l) + \right.$$
$$\left. \left. + \sum_{m=1}^{2n-2} f_s^h(x_+,n) f_{qq,q,s}^h(x_-,n_m) \right] \right\} ,$$

where $V_{pA}^{(\nu)}$ is the probability of "pure inelastic" (nondiffractive) interactions with ν target nucleons, and we should account for all possible Pomeron permutation and the difference in quark content of the protons and neutrons in the target.

In particular, the contribution of the diagram in Fig. 2 to the inclusive spectrum is

$$\frac{x_E}{\sigma_{pA}^{prod}}\frac{d\sigma}{dx_F} = 2V_{pA}^{(2)} w_1^{pN_1} w_2^{pN_2} \left\{ f_{qq}^h(x_+,3) f_q^h(x_-,1) + \right. \tag{6}$$
$$+ f_q^h(x_+,3) f_{qq}^h(x_-,1) + f_s^h(x_+,3) [f_{qq}^h(x_-,2) + f_q^h(x_-,2) +$$
$$\left. + 2 f_s^h(x_-,2)] \right\} .$$

The diquark and quark distributions as well as the fragmentation functions are here the same as in the case of a nucleon target.

3 Inclusive spectra in heavy ion collisions at intermediate energies

At comparatively low energies we do not have a simple model for the calculation of the yields of secondaries. However, there exist the data [15, 16], which show that the yields of secondaries produced by one interacting nucleon increase with the increase of the number of interacting nucleons. An example is presented in Fig. 3 taken from [16].

It is clear that the increase of the number of projectile participant, N_{part}, means the decrease of the impact parameter and every participant interacts, on the average, with larger number of target nucleons, ν_{NA} [26]. One can see from Fig. 3 that every projectile nucleon produces more both K^+ and K^- at small impact parameters in comparison with peripheral interactions. These ratios change about 2–2.5 time from large to small impact parameters[1]. It means that the multiplicity of the produced kaons is a real function of ν_{AB}, that is the number of elementary nucleon–nucleon collisions in the case of inelastic interaction of nucleus A with nucleus B and

$$\langle \nu_{AB} \rangle = \frac{AB\sigma_{NN}^{inel}}{\sigma_{AB}^{prod}} . \tag{7}$$

[1]Due to the energy correction factors [22] these ratios should not be equal exactly to ν_{NA}

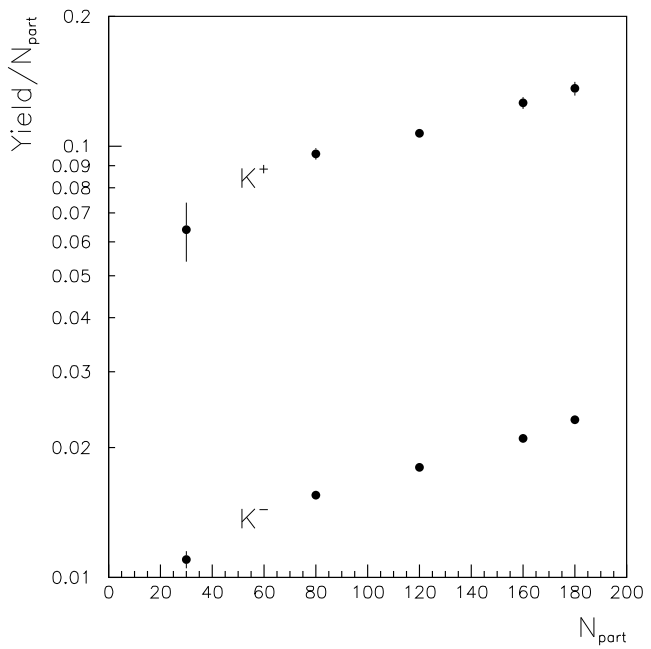

Fig. 3. The total yields of kaons per projectile participant versus the number of projectile participants N_{part} in $Au - Au$ reactions at 11.6A GeV/c.

This fact confirms the applicability of the Multiple Scattering Theory at the energies of GSI, as a minimum.

The similar situation probably takes place at CERN SPS energies, see Fig. 10 in [17]. The saturation of the yields of secondaries produced by one interacting nucleon possibly can be seen only at $N_{pp} > 300$, i.e. in very central events. However, it is necessary to note that the data [17] are in some disagreement with the data [18].

At CERN SPS energies 158A GeV/c, following to the data [17], we can use the QGSM and calculate the spectra of secondaries. In the case of heavy ion collisions the energy conservation effects violate the asymptotical ratio

$$\frac{1}{\sigma_{AB}^{prod}}\frac{d\sigma(AB \to hX)}{dy} = \langle \nu_{AB} \rangle \frac{1}{\sigma_{NN}^{inel}}\frac{d\sigma(NN \to hX)}{dy} \tag{8}$$

significantly stronger than in the case of hadron–nucleus collisions, where the asymptotical value is

$$\frac{1}{\sigma_{NA}^{prod}}\frac{d\sigma(NA \to hX)}{dy} = \langle \nu_{NA} \rangle \frac{1}{\sigma_{NN}^{in}}\frac{d\sigma(NN \to hX)}{dy} \tag{9}$$

with

$$\langle \nu_{NA} \rangle = \frac{A\sigma_{NN}^{inel}}{\sigma_{NA}^{prod}} \ . \tag{10}$$

The possible way to account for the energy conservation effects was suggested in [27]. The idea is that we will use the rigid target approximation in two different ways. In the case of forward hemisphere (nucleus A fragmentation region) we account for that each nucleon of the nucleus A can interact with several nucleons of the nucleus B, but the nucleons of B interact not more than once. This is equivalent to the case, where A uncoupled nucleons, with the corresponding impact parameter distribution, interact with the nucleus B. In the backward hemisphere (nucleus B fragmentation region) we will use the same, but with change A and B. Now B uncoupled nucleons interact with the nucleus A. The two contributions in the central region are matched with good accuracy.

The inclusive spectrum of secondaries produced in $A-B$ collision can be written as

$$\begin{aligned} \frac{1}{\sigma_{AB}^{prod}} \frac{d\sigma(AB \to hX)}{dy} &= \theta(y) R_A^h(y) \langle N_A \rangle \frac{1}{\sigma_{NB}^{prod}} \frac{d\sigma(NB \to hX)}{dy} + \\ &+ \theta(-y) R_B^h(-y) \langle N_B \rangle \frac{1}{\sigma_{NA}^{prod}} \frac{d\sigma(NA \to hX)}{dy} \ , \end{aligned} \tag{11}$$

where y is the rapidity of secondary h in c.m. frame and the functions $R_{A,B}^h(y)$ account for the energy conservation effects.

Here we connect the inclusive spectra of secondaries in the heavy ion collisions with the spectra in the nucleon–nucleus interactions. To calculate the last ones, as well as the functions $R_{A,B}^h(y)$ we use QGSM and the Multiple Scattering Theory for NA collisions [5].

The functions $R_{A,B}^h(y)$ can be taken in the form [27]

$$R_A^h(y) = \frac{f^h(-y, \langle \nu \rangle_{NA})}{\langle \nu \rangle_{NA} f^h(-y, 1)} \ , \tag{12}$$

where $f^h(y, \nu)$ is the contribution to the secondary h spectrum from a beam nucleon interaction with ν target nucleons, and $f^h(y, 1)$ is the spectrum of secondary particle h in NN collision.

The rapidity distributions of secondary π^-, K^+ and K^- [29], as well as π^+, p and $\bar{p}$ [17] measured in $Pb-Pb$ central collisions at 158 GeV/c per nucleon are compared with our calculations using Eq. (11) in Fig. 4.

In the case of pions the agreement is reasonable. The differences between the calculated curves and the data are not larger than 10%. In the case of secondary kaons we see that there is a problem. The spectrum of K^- also is in reasonable agreement with the model, whereas for K^+ disagreement is about 30%. Even more serious is the K^+/K^- ratio. Experimentally this ratio at $y \sim 0$ is about 1.5, however in the model we can not

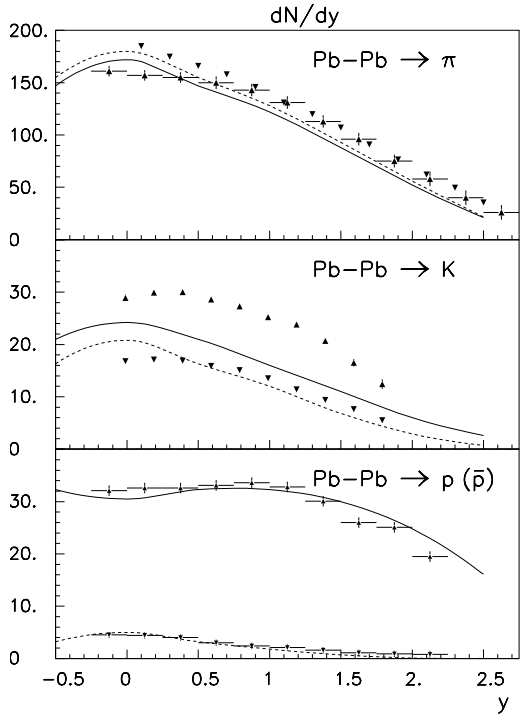

Fig. 4. The rapidity distributions of secondary π^+, π^-, K^+, K^-, p and $\bar{p}$ produced in the central $Pb-Pb$ collisions at 158 GeV/c per nucleon. Triangles show the results for the positive secondaries and over turned triangles for the negative ones. The solid curves are the QGSM predictions for positive secondaries and dashed curves for the negative ones.

obtain more than 1.2, the ratio about 1.5 being obtained for pp collisions at the discussed energy. Most probably it means that the difference between fragmentation functions of diquarks and/or quarks into K^+ and K^- is not large enough in the model. The used fragmentation functions were taken from [2]. In the cases of p and $\bar{p}$ the agreement with the data is good enough. The contribution from string junction diffusion [30]-[33] to the proton spectrum is small at this energy.

4 Inclusive spectra at high energies

The Multiple Scattering Theory allows one to obtain some simple and model independent formulae [34, 35] coming only from the assumption that high energy heavy ion collision can be consider as the superposition of independent nucleon-nucleon collisions. So any serious disagreement of these predictions with the data can be considered as the signal for some collective interaction.

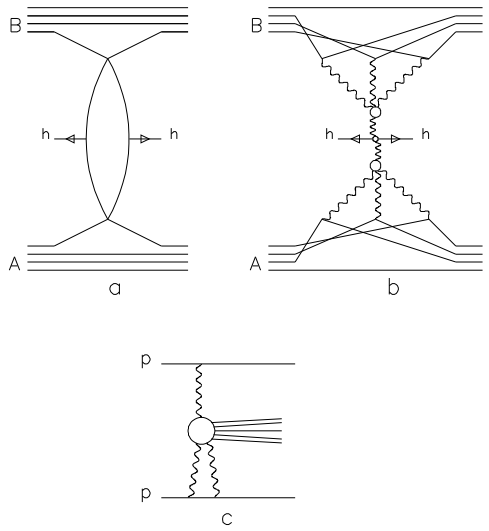

Fig. 5. Diagrams for inclusive cross sections for $A-B$ collisions in Glauber approximation (a) and with accounting for the interactions of pomerons (shown by wave curves) (b). An example of inelastic processes of pp interactions which determine one of the vertices of the multipomeron interactions (c).

The predictions for rapidity spectra of secondaries are more model dependent. The RHIC experimental data give clear evidences for the effects of inclusive density saturation, which reduce the inclusive density about two times in the central (midrapidity) region in comparison, say, with predictions of [36, 37] based on the superposition picture. The observed phenomena can be explained in the framework of the space–time picture of high energy interactions and on Gribov's Reggeon diagram technique [38]. In high energy hadron–nucleus collision there exists inelastic screening corrections [39, 40]. The same inelastic screening should exist in high energy heavy ion collision. This effect is very small for integrated cross sections (because many of them are determined by geometry), but it is very important [19] for the calculations of secondary multiplicities and inclusive densities.

At not very high energies the heavy ion collisions can be considered with the help of standard Glauber approximation, and the inclusive spectrum of any secondary h produced in the central region is described by the diagram shown in Fig. 5a, i.e. by the contribution of a single nucleon–nucleon blob. This diagram immediately gives Eq. (11) (and Eq. (12) after accounting the corrections for finite energy) for heavy ion inclusive cross section. The contributions of all other diagrams cancel each other due to AGK cutting rules [8].

At high energies the new diagrams appear, which include the interactions of pomerons and correspond to the diffractive production of a large mass M jet in pp interactions.

At low energies the contribution of such diagrams to nucleus–nucleus interaction is suppressed by the longitudinal part of nuclear form factor $G_z(t_{min})$ which is connected with the longitudinal part of momentum transfer, q_z ($t_{min} = -q_z^2$). Thiz longitudinal form factor can be written for Gaussian distribution of nuclear density $\rho(b,z)$ as

$$G_A(t_{min}) = \int \rho_A(b,z) e^{iq_z z} dz \approx \exp\left(R_A^2 t_{min}/3\right) . \tag{13}$$

When energy becomes high enough, the value of t_{min} becomes very small. So the discussed contribution can be significant.

One example of a diagram with pomeron interaction for heavy ion interaction is shown in Fig. 5b. Contrary to the hadron–nucleus case, where the inelastic screening is connected with the diffractive dissociation of projectile particle [39, 40], the contribution of such diagram can be estimated from the processes of high mass jet production in midrapidity region and with two large rapidity gaps, see for example Fig. 5c. The contribution of the considered diagrams to inclusive spectrum is suppressed quadratically, by both longitudinal form factors, $G_A(t_{min})$ and $G_B(t_{min})$. So we can observe their influence at energies quadratically higher in comparison with the energies region, where the inelastic screening effects are observed in hadron–nucleus scattering.

Following to the estimations of [19], the RHIC energies are of the needed order of magnitude. The inelastic screening can decrease [19] the inclusive density in the midrapidity region about two times at RHIC energies and about three times at LHC energies in comparison with the calculation without inelastic screening.

However all such estimation are model dependent. The numerical contribution of all multipomeron diagrams is rather unclear due to a lot of unknown vertices for the multipomeron interactions, and the number of multipomeron diagrams is very large. The number of parameters can be decreased in some model, for example, in [19] the Schwimmer model [41] was used for the numerical estimations.

Another (again model dependent) possibility to estimate the contribution of the diagrams with Pomeron interaction comes [42, 43, 44] from percolation theory. In this approach we assume that if two or several pomerons are overlapping, they become a one pomeron. When all Pomerons are overlapping, the inclusive density is saturated, it reaches its maximal value at given impact parameter. This approach has one free parameter - the critical number of pomerons in one squared fermi. Technically it is more simple to bound the maximal number of pomerons, n_{max}, which can be emitted by one participating nucleon for the given pair of colliding nuclei. All model calculations become rather simple because above the critical value every additional pomeron cannot contribute to the inclusive spectrum.

The results of calculations of the inclusive densities of the produced charged secondaries per one pair on interacting nucleons $dn_{ch}/dy/(0.5N_{part})$, with the help of Eq. (11) and QGSM are shown in Fig. 6. We present the CERN SPS experimental data for $Pb-Pb$ collisions at $\sqrt{s} = 17.3$ GeV per nucleon [45]-[48] for $|y| < 1$ and RHIC data for $Au-Au$ at $\sqrt{s} = 130$ GeV per nucleon [48, 49] (these data are in agreement with the results of more recent measurements).

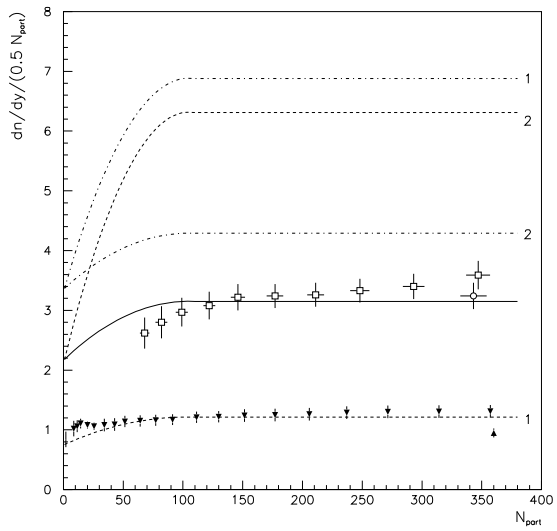

Fig. 6. Relative inclusive densities of secondaries for $Pb-Pb$ collisions at $\sqrt{s}=17.3$ GeV per nucleon (black points, multiplied by 1/2) and for $Au-Au$ at $\sqrt{s}=130$ GeV per nucleon (open points). Dashed curves present the QGSM results without percolation effects for $\sqrt{s}=17.3$ GeV (curve 1, multiplied by 1/2, as the points) and for $\sqrt{s}=130$ GeV (curve 2). The solid curve shows the results of calculations at $\sqrt{s}=130$ GeV with percolation effects ($\langle n_{max}\rangle=1.67$). Dash–dotted curves 1 and 2 show the predictions for $Pb-Pb$ collisions at 5.5 TeV per nucleon with $\langle n_{max}\rangle=1.67$ and $\langle n_{max}\rangle=1$, respectively.

One can see that CERN SPS data at $\sqrt{s}=17.3$ GeV are described reasonably (dashed curve 1 in Fig. 6) without any additional screening corrections, by the same way as the results shown in Fig. 4 for different secondary hadrons. It seems to be natural because the suppression effects of t_{min}, Eq. (13), discussed above should be very important at comparatively low energy of CERN SpS.

However, the same calculation at RHIC energy $\sqrt{s}=130$ GeV per nucleon gives the relative inclusive density two times larger (dashed curve 2 in Fig. 6) than the data. The agreement with the data can be obtained only with suppression of multipomeron contributions, namely by using $\langle n_{max}\rangle=1.67$ for every interacting nucleons. In this case the averaged number of cutted Pomerons emitted by every interacting nucleon is about 1.2 that is significantly smaller than the number of cutted Pomerons in pp collisions at the same energy (the last one is about 1.8).

Here we assume that the value $\langle n_{max}\rangle$ does not depends on N_{part} in the interval $A/4<N_{part}<A$, i.e. between minimum bias and very central collisions [26]. This assumption, as one can see from Fig. 6, is in agreement with the presented RHIC experimental data with the accuracy 10-20 %. It is confirmed (within the same accuracy) by the recent data [50] that the ratio of charged particle multiplicities in central (where $N_{part}\approx A$) $Au-Au$ and $Cu-Cu$ collisions in midrapidity region are both at $\sqrt{s}=200$ GeV and 62.4 GeV only 15 % large that the ratio of Au and Cu atomic weights. However, it is necessary to note that the calculated inclusive densities in heavy ion collisions per one

pair of participants are about 1.6 times larger than in pp collisions.

The same value of $\langle n_{max} \rangle = 1.67$ allows us [51] to describe the PHOBOS point at $\sqrt{s} = 56$ GeV [48]. It means, that the saturation effects at $\sqrt{s} = 56$ GeV are of the same order of magnitude as at $\sqrt{s} = 130$ GeV and 200 GeV.

The result of PHOBOS Coll. [52] for central $Au - Au$ collisions at $\sqrt{s} = 200$ GeV per nucleon gives $dn_{ch}/d\eta = 650 \pm 35$ for $|\eta| < 1$ that is in agreement with our result $dn_{ch}/d\eta \approx 600$. The important point is that the experimental data [53] of NA50 Coll. for central $Pb - Pb$ collisions show the increase of the multiplicities of secondaries, $dn_{ch}/d\eta$, in the energy interval $\sqrt{s} = 8.8$ GeV – 17.3 GeV about two times, from $207 \pm 1 \pm 16$ to $428 \pm 1 \pm 34$. In the much larger (in logarithmical scale) interval $\sqrt{s} = 17.3$ GeV – 200 GeV these multiplicities increase only about 1.5 times. Probably it means that the inelastic screening (percolation) effects start to work at energies about $\sqrt{s} \sim 20 - 30$ GeV and they become very significant at $\sqrt{s} \sim 50$ GeV.

More detailed data are presented in [54] and in [55], where the multiplicities of identified hadrons were measured in $Au - Au$ at $\sqrt{s} = 130$ GeV and 200 GeV, respectively. The values of $dn/dy/(0.5N_{part})$ for different secondaries produced in 5 % of the most central $Au - Au$ interaction are compared with our QGSM calculations in the Table. Percolation effects were accounted for, as it was explained above. The agreement of the QGSM calculations with the data is on the level of 20 % that is usual for QGSM (let us note that we did not input any new parameter). In particular, one can see qualitative agreement of the calculated results and the data in the energy dependences of midrapidity multiplicities for secondary pions and kaons, but rather strange disagreement for secondary protons and antiprotons.

Table

The values of $dn/dy/(0.5N_{part})$ for different secondaries produced in 5 % of the most central $Au - Au$ collisions at $\sqrt{s} = 130$ GeV and 200 GeV.

Hadron	130 GeV		200 GeV	
	[54]	QGSM	[55]	QGSM
π^+	1.59 ± 0.05	1.82	1.63 ± 0.13	2.00
π^-	1.55 ± 0.05	1.88	1.61 ± 0.13	2.05
K^+	0.27 ± 0.02	0.17	0.28 ± 0.04	0.19
K^-	0.23 ± 0.02	0.17	0.26 ± 0.04	0.18
p	0.16 ± 0.01	0.13	0.10 ± 0.01	0.14
$\bar{p}$	0.11 ± 0.01	0.08	0.08 ± 0.01	0.10

The results of Dual String Model [56, 57] calculations with string fusion [51] are in agreement with the results of the percolation model. The results [58] of String Fusion Model [59] are also in agreement with presented calculations.

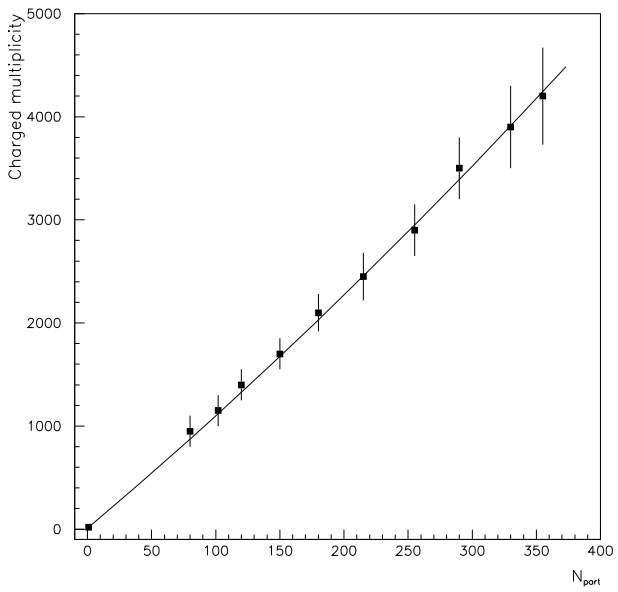

Fig. 7. Total number of charged particles detected within range $-5.4 < \eta < 5.4$ in $Au - Au$ collisions at $\sqrt{s} = 130$ GeV per nucleon as a function of N_{part} and its description by the QGSM with percolation effects and $\langle n_{max} \rangle = 1.67$ solid curve.

In the case of LHC energy $\sqrt{s} = 5.5$ TeV per nucleon for $Pb - Pb$ collisions with $\langle n_{max} \rangle = 1.67$ percolation effect decreases the relative inclusive density about 3 times. This result is shown by dash-dotted curve 1 in Fig. 6 and it is again similar to [19] prediction. Let us note that the energy difference in calculations with and without percolation effects is connected mainly with the increase of the total inelastic NN cross section.

However, the percolation effect at LHC energy can be even larger if the increase of the transverse range of a pomeron with incident energy will be accounted for [51]. The predictions for the relative inclusive density at LHC energy with $\langle n_{max} \rangle = 1$ (maximal percolation) are shown in Fig. 6 by dash-dotted curve 2. Now the percolation effect decreases the relative inclusive density about 5 times.

The data [60] on the total number of charged particles detected within range $-5.4 < \eta < 5.4$, i.e. in the region which exclude only high-x_F fragmentation and diffraction regions are presented in Fig. 7.

These data are in good agreement with the QGSM calculations accounting for the percolation effects. The calculated dependence are very close to a straight line that is the direct consequence of Eq. (11).

5 Conclusion

We can see that the QGSM together with Multiple Scattering Theory can describe on reasonable level the inclusive spectra of different secondaries produced in heavy ion collisions at not very high energies. Some disagreement in K^+ and K^- yields in Fig. 4

can be corrected by reasonable change of the diquark and quark fragmentation functions into different kaons.

The data of RHIC and their comparison with CERN SPS data show numerically large effects coming from the Pomeron (secondary particle) density saturation. It is the first experimental evidence of so numerically large effects in high energy physics. The inelastic screening effects should be accounted for in calculations of inclusive spectra of different secondaries produced in heavy ion collisions at RHIC and LHC energies. The processes of baryon number transfer via string junction diffusion [30]–[33] also should be accounted at these energies.

From the comparison of the RHIC data (where effects are large) and CERN SPS data (where effects are small) we can conclude that the inelastic screening (saturation effects) become very important for heavy ion collisions in the energy interval $\sqrt{s_{NN}} =$ 20 - 30 GeV and they, probably, are saturated at $\sqrt{s_{NN}} = 60$ GeV. At higher energies the growth of total inelastic NN cross section results in the increase of the number of Pomerons which can be screened, so the difference in calculations with and without inelastic shadowing becomes larger.

We are grateful to N. Armesto, A. Capella, C. Pajares and R. Ugoccioni for useful discussions. This paper was supported, in part, by grants RSGSS-1124.2003.2 and PDD (CP) PST.CLG980287.

References

[1] A. B. Kaidalov, K. A. Ter–Martirosyan, Yad. Fiz. **39**, 1545 (1984); **40**, 211 (1984).

[2] A. B. Kaidalov, O. I. Piskunova, Yad. Fiz. **41**, 1278 (1985).

[3] A. Capella, U. Sukhatme, C. I. Tan, J. Tran Thanh Van, Phys. Rep. **236**, 225 (1994).

[4] A. Capella, J. Tran Thanh Van, Z. Phys. C**10**, 249 (1981).

[5] A. B. Kaidalov, K. A. Ter-Martirosyan, Yu. M. Shabelski, Yad. Fiz. **43**, 1282 (1986).

[6] Yu. M. Shabelski, Yad. Fiz. **44**, 186 (1986).

[7] Yu. M. Shabelski, Nucl. Phys. Proc. Suppl. **52B**, 116 (1997).

[8] V. A. Abramovsky, V. N. Gribov, O. V. Kancheli, Yad. Fiz. **18**, 595 (1973).

[9] A. B. Kaidalov, Sov. J. Nucl. Phys. **45**, 902 (1987); Yad. Fiz. **43**, 1282 (1986).

[10] W. Czyz and L. G. Maximon, Ann. Phys. **52**, 59 (1969).

[11] G. D. Alkhazov et al., Nucl. Phys. **A220**, 365 (1977).

[12] I. V. Andreev and A. V. Chernov, Yad. Fiz. **28**, 477 (1978).

[13] M. A. Braun, Yad. Fiz. **45**, 1625 (1987).

[14] K. G. Boreskov and A. B. Kaidalov, Yad. Fiz. **48**, 575 (1988).

[15] L. Ahle et al., Nucl. Phys. **A610**, 139c (1996).

[16] L. Ahle et al., Phys. Rev. **C58**, 3523 (1998).

[17] F. Sikler et al., NA49 Coll., Nucl.Phys. **A661**,45c (1999).

[18] S. Kabana et al., NA52 Coll., Nucl.Phys. **A661**, 370c (1999).

[19] A. Capella, A. Kaidalov and J. Tran Thanh Van, Heavy Ion Phys. **9**, 169 (1999).

[20] G. C. Rossi, G. Veneziano, Nucl. Phys. B**123**, 507 (1977).

[21] K. A. Ter–Martirosyan, Phys. Lett. **44B**, 377 (1973).

[22] Yu. M. Shabelski, Yad.Fiz. **26**, 1084 (1977); Nucl. Phys. **B132**, 491 (1978).

[23] L. Bertocchi and D. Treleani, J. Phys. **G3**, 147 (1977).

[24] J. Weis, Acta Phys. Polonica **B7**, 85 (1977).

[25] T. Jaroszewicz et al., Z. Phys. **C1**, 181 (1979).

[26] C. Pajares and Yu. M. Shabelski, Yad. Fiz. **63**, 980 (2000).

[27] Yu. M. Shabelski, Acta Phys. Polonica **B10**, 1049 (1979).

[28] Yu. M. Shabelski, Yad. Fiz. **50**, 239 (1989).

[29] S. V. Afanasiev et al., NA49 Coll. Phys. Rev. **C66**, 054902 (2002).

[30] G. H. Arakelyan, A. Capella, A. B. Kaidalov and Yu. M. Shabelski, Eur. Phys. J. **C26**, 81 (2002); hep-ph/0103337.

[31] F. Bopp and Yu. M. Shabelski, Yad. Fiz. **68**, 2155 (2005); hep-ph/0406158.

[32] F. Bopp and Yu. M. Shabelski, Eur. Phys. J. **A28**, 237 (2006); hep-ph/0603193.

[33] G. H. Arakelyan, C. Merino and Yu. M. Shabelski, Yad. Fiz. **69**, 911 (2006); hep-ph/0505100.

[34] C. Pajares and A. V. Ramallo, Phys. Rev. **C16**, 2800 (1985).

[35] V. M. Braun and Yu. M. Shabelski, Int. J. of Mod. Phys. **A3**, 2417 (1988).

[36] A. Capella, C. Merino and J. Tran Thanh Van, Phys. Lett. **B265** (1991) 415.

[37] Yu. M. Shabelski, Z. Phys. **C57**, 409 (1993).

[38] V. N. Gribov, ZhETF **53**, 654 (1967).

[39] V. N. Gribov, ZhETF **56**, 892 (1968).

[40] V. N. Gribov, ZhETF **57**, 1306 (1969).

[41] A. Schwimmer, Nucl. Phys. **B94**, 445 (1975).

[42] J. Dias de Deus, R. Ugoccioni and A. Rodrigues, Phys. Lett. **B458**, 402 (1999); Eur. Phys. J. **C16**, 537 (2000).

[43] M. A. Braun and C. Pajares, Phys. Rev. Lett. **85**, 4864 (2000).

[44] J. Dias de Deus and Yu. M. Shabelski, Eur. Phys. J. **A20**, 457 (2004).

[45] NA49 Coll. P. Jones et al., Nucl. Phys. **A610**, 188c (1996).

[46] NA49 Coll. H. Appelshauser et al., Phys. Rev. Lett. **82**, 2471 (1999).

[47] WA98 Coll. M. M. Aggarwal et al., Eur. Phys. J. **C18**, 651 (2001).

[48] PHOBOS Coll. B. B. Back et al., Phys. Rev. Lett. **85**, 3100 (2000).

[49] PHENIX Coll. K. Adcox et al., Phys. Rev. Lett. **86**, 3500 (2001).

[50] PHOBOS Coll. B. B. Back et al., nucl-ex/0604017.

[51] J. Dias de Deus, Yu. M. Shabelski and R. Ugoccioni, hep-ph/0108253.

[52] PHOBOS Coll. B. B. Back et al., Phys. Rev. Lett. **88**, 022302 (2002); nucl-ex/0108009.

[53] NA50 Coll. M. C. Abreu et al., Phys. Lett. **B530**, 33 (2002).

[54] PHENIX Coll. A. Adcox et al., Phys. Rev. **C69**, 024904 (2004); nucl-ex/0307010.

[55] PHENIX Coll., S. S. Adler et al., Phys. Rev. **C69**, 034909 (2004); nucl-ex/0307022.

[56] J. Dias de Deus and R. Ugoccioni, Phys. Lett. **B491**, 253 (2000).

[57] J. Dias de Deus and R. Ugoccioni, Phys. Lett. **B494**, 53 (2000).

[58] N. Armesto, C. Pajares and D. Sousa, Phys. Lett. **B527**, 92 (2002); hep-ph/0104269.

[59] N. S. Amelin, M. A. Braun and C. Pajares, Phys. Lett. **B306**, 312 (1993); Z.Phys. **C63**, 507 (1994).

[60] PHOBOS Coll. B. B. Back et al., Phys. Rev. Lett. **87**, 102303 (2001); nucl-ex/0106006.